Available online at www.sciencedirect.com
SCIENCE DIRECT®
ELSEVIER
Earth and Planetary Science Letters 236 (2005) 388–403
EPSL
www.elsevier.com/locate/epsl

Comparison of U–Th, paleomagnetism, and cosmogenic burial methods for dating caves: Implications for landscape evolution studies

Greg M. Stock[a,*], Darryl E. Granger[b], Ira D. Sasowsky[c], Robert S. Anderson[d], Robert C. Finkel[e]

[a]*Department of Earth Sciences, University of California, Santa Cruz, CA 95064, USA*
[b]*Department of Earth and Atmospheric Sciences, Purdue University, West Lafayette, IN 47907, USA*
[c]*Office for Terrestrial Records of Environmental Change, Department of Geology and Center for Environmental Studies, University of Akron, Akron, OH 44325, USA*
[d]*Department of Geological Sciences and Institute of Arctic and Alpine Research, University of Colorado, Boulder, CO 80309, USA*
[e]*Center for Accelerator Mass Spectrometry and Geosciences and Environmental Technology, Lawrence Livermore National Laboratory, Livermore, CA 94550, USA*

Received 10 November 2004; received in revised form 3 April 2005; accepted 18 April 2005
Available online 22 June 2005
Editor: K. Farley

Abstract

Caves are useful in landscape evolution studies because they often mark the level of previous water tables and, when dated, yield incision rates. Dating caves is problematic, however, because their ages are only constrained by the oldest deposits contained within, which may be far younger than the cave itself. We dated cave deposits in the Sierra Nevada using U–Th dating of speleothems, paleomagnetic dating of fine sediment, and cosmogenic $^{26}Al/^{10}Be$ burial dating of coarse sediment. The sampled caves formed sequentially as the water table lowered, providing an important stratigraphic test for the dating methods. Large discrepancies between deposit ages from similar cave levels demonstrate that, even when accurately determined, deposit ages can seriously underestimate the timing of cave development. Drip-type speleothems are most prone to this minimum age bias because they can accumulate long after caves form, and because the U–Th method is limited to ~400 ka. Paleomagnetic dating requires correlation with the global reversal chronology, and is hindered by a lack of continuous stratigraphy. The fine sediment analyzed for paleomagnetism is also highly susceptible to remobilization and deposition in cave passages well above base level. Cosmogenic $^{26}Al/^{10}Be$ dates bedload material deposited when caves were at or very near river level, and can date material as old as ~5 Ma. In the Sierra Nevada, speleothem U–Th ages and sediment burial ages from the same cave levels differ by as much as an order of magnitude. These results suggest speleothem ages alone may significantly underestimate cave ages

* Corresponding author. Present address: Department of Geological Sciences, University of Michigan, Ann Arbor, MI 48109-1005, USA, Tel.: +1 734 615 4076.
E-mail addresses: gstock@umich.edu (G.M. Stock), dgranger@purdue.edu (D.E. Granger), ids@uakron.edu (I.D. Sasowsky), andersrs@colorado.edu (R.S. Anderson), finkel1@llnl.gov (R.C. Finkel).

0012-821X/$ - see front matter
doi:10.1016/j.epsl.2005.04.024

and thereby overestimate rates of landscape evolution. Cosmogenic burial dating of coarse clastic sediment appears to be the most reliable method for dating cave development in mountainous regions.

Keywords: geochronology; Uranium-series; paleomagnetism; cosmogenic nuclides; caves; landscape evolution; Sierra Nevada

1. Introduction

Landscape evolution studies require dated geomorphic markers to document long-term erosion rates and reconstruct past landforms. Examples of such markers include fluvial or strath terraces, volcanic deposits, and erosional surfaces (e.g., [1–5]). However, geomorphic markers are commonly absent from rapidly eroding landscapes such as mountain belts, either because conditions were not conducive to their development, or because they were destroyed by erosion after they formed. Where markers are present, determining their age frequently poses a serious challenge.

Caves may be useful geomorphic markers because their development is often tied to river position, and because they are frequently located in landscapes lacking terraces or other markers. Although caves are limited to landscapes underlain by carbonate rock, such landscapes represent ~12% of the Earth's ice-free land surface [6], and are relatively common in mountainous regions. Certain caves can record landscape changes because they form at the water table and are subsequently left perched in valley walls as local base level is lowered by bedrock incision. When dated, these caves provide rates of incision, the primary erosional process governing the pace at which landscapes evolve (e.g., [7–15]).

Archeological, paleontological, and paleoclimatological studies seek to date specific deposits within caves (e.g., [16–18]). Landscape evolution studies differ somewhat because they seek the age of the cave itself. This poses a unique challenge for geochronology, as caves are voids that cannot be directly dated [19]. Although in certain rare cases Ar–Ar dating of clays produced during hydrothermal-related sulfuric acid dissolution can directly date cave development [20], this dissolution mechanism is limited to only a few sites globally. Far more common are caves formed by carbonic acid dissolution [6,21], whose ages must be younger than their host bedrock and older than materials deposited within them. As most caves are much younger than their host bedrock, cave ages are usually constrained by dating either clastic sediment carried into the cave by fluvial processes, or calcite speleothems formed in situ by meteoric drip water. Speleothems may be dated by U-series (typically ^{234}U–^{230}Th), and sediment by paleomagnetism and cosmogenic $^{26}Al/^{10}Be$ burial dating.

Any cave deposit necessarily postdates cave development, so deposit ages provide only minimum ages for cave development [7,19]. Correspondingly, rates of incision based on cave ages must be considered maximum rates [7,8]. The degree to which sediment and speleothem deposition accurately captures the timing of cave development has not previously been explored in detail. Here we compare ages for cave deposits in the Sierra Nevada, California, determined by U–Th, paleomagnetic, and cosmogenic burial dating. While each dating method has limitations, our results suggest that both speleothem U–Th dating and fine sediment paleomagnetism are particularly susceptible to potentially large systematic biases in cave age.

2. Cave development and landscape evolution

Cave passages form by dissolution of carbonate rock along paths of greatest groundwater discharge. Vadose passages form above the water table and typically consist of narrow, sinuous, and often steeply dipping canyon passages, while phreatic passages form at or below the water table and typically consist of tubes with rounded cross sections [21]. Although deep phreatic passages can form well below the water table, their U-shaped longitudinal profiles are distinct from the low-gradient profiles of shallow phreatic tubes formed along water table surfaces [6,21,22]; these latter passages are most useful in cave-based landscape evolution studies. The simplest caves form when portions of rivers are briefly diverted into canyon walls, dissolving phreatic passages parallel to canyon walls (Fig. 1, left). Alternatively, sinking tributary streams dissolve cave passages along water table surfaces graded to river level (Fig. 1,

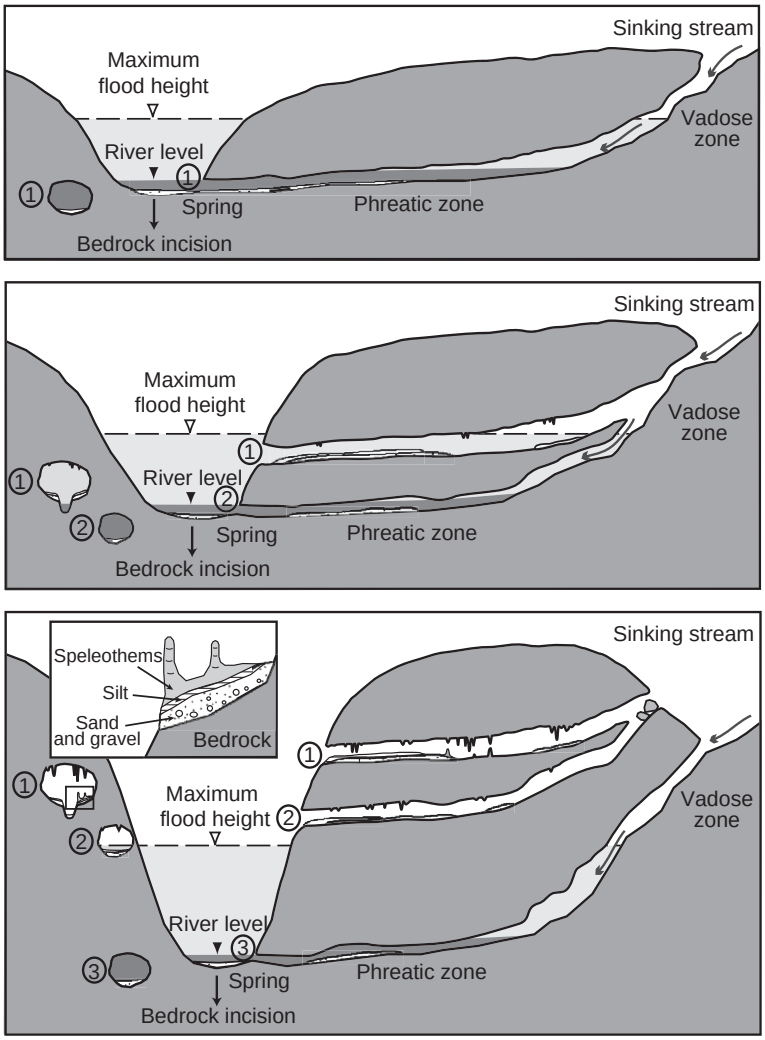

Fig. 1. Cave development in an incising landscape. Left side shows caves forming parallel to river, right side shows cave development by sinking tributary stream graded to river level. Numbers correspond to periods of cave development; bedrock incision leaves progressively older cave levels perched in canyon walls. Coarse sediment is deposited when caves are at, or very near, river level. Fine-grained sediment can be deposited throughout the interval that caves are within the zone of maximum flood height. Speleothems can form anytime after phreatic waters drain from cave passages, but accumulate most readily after fluvial activity has ceased. Inset shows resulting cave deposit stratigraphy.

right). Cave passages fed by sinking streams usually contain both a vadose upstream section and a phreatic downstream section, with the transition point marking the former water table level [22]. Groundwater moving through cave passages eventually emerges as springs at river level. When river position is stable for long periods, these springs remain at a fixed elevation and large phreatic passages form. Subsequent incision lowers the local water table, diverting groundwater to a lower level and exposing phreatic passages (Fig. 1).

During the waning stages of cave development, coarse sediment often moves through caves as bedload. We argue that, except in unusual cases, very coarse sediment (e.g., coarse sand, gravel, cobbles) is mobilized only when caves are at or very near river level. As bedrock incision progresses, this coarse sediment remains in passages abandoned by groundwater. In contrast, subsequent floodwaters can easily remobilize previously deposited fine sediment (e.g., silt, clay), and can also waft suspended load into upper level passages

(Fig. 1), leaving fine sediment draped over coarse sediment [23]. Once rivers incise sufficiently far that cave passages are no longer subjected to even large floods, accumulation of drip-type speleothems (e.g., stalactites, stalagmites, flowstone) dominates, capping both coarse and fine sediments. Drip-type speleothems cannot form in active phreatic conduits, but they may form anytime after groundwater drains from these passages. Thus, a commonly found cave deposit consists of coarse sediment resting on bedrock, an overlying fine sediment deposit, and a capping speleothem layer (Fig. 1 inset).

For incising river systems, the conceptual model of cave development outlined above dictates two stratigraphic settings relevant to dating studies: 1) a canyon wall stratigraphy, in which cave ages *increase* upward, and 2) a cave deposit stratigraphy, in which deposit ages *decrease* upward [10]. This model provides a critical test for dated cave deposits used to infer cave ages. Barring major aggradation of the river, cave ages inferred from the oldest deposits should increase with height above modern river levels if they accurately record the timing of cave development. Deposit ages from the same cave level should be similar. Within a specific deposit, stratigraphic unit ages should decrease with height above the bedrock base of the deposit.

3. Methods of determining cave ages

3.1. U–Th speleothem dating

Drip-type speleothem ages provide the chronology for most work using caves to derive landscape evolution rates (e.g., [7,8,24–26]). Uranium-series dating of speleothems is a well-established technique reviewed in detail elsewhere (e.g., [27–29]). Most speleothem dating studies utilize disequilibrium in the ^{238}U–^{234}U–^{230}Th system, in which the $^{230}Th/^{238}U$ activity ratio, $[^{230}Th/^{238}U]_{Act}$, approaches unity as a function of time t:

$$\left[\frac{^{230}Th}{^{238}U}\right]_{Act} = 1 - e^{-\lambda_{230}t} + \left(\left[\frac{^{234}U}{^{238}U}\right]_{Act} - 1\right) \times \left(\frac{\lambda_{230}}{\lambda_{230}-\lambda_{234}}\right)\left(1 - e^{-(\lambda_{230}-\lambda_{234})t}\right) \quad (1)$$

where λ_{230} and λ_{234} are decay constants [30] Eq. (1) assumes all measured ^{230}Th derives from decay of ^{234}U. In fact, initial ^{230}Th may be present, usually associated with detrital sediment imbedded in the calcite. Initial ^{230}Th is best addressed using total dissolution isochron methods (e.g., [28,29]), but a first-order correction can be made by assuming that ^{230}Th associated with ^{232}Th was incorporated into speleothem calcite during deposition and has decayed over time t since then. The radiogenic ^{230}Th derived from ^{238}U, $[^{230}Th^*/^{238}U]_{Act}$, can then be calculated using Eq. (2):

$$\left[\frac{^{230}Th^*}{^{238}U}\right]_{Act} = \left[\frac{^{230}Th}{^{238}U}\right]_{Act_m} - \left[\frac{^{232}Th}{^{238}U}\right]_{Act} R_o e^{-\lambda_{230}t} \quad (2)$$

where R_0 is the initial $[^{230}Th/^{232}Th]$ activity ratio in the detritus at the time of speleothem deposition and subscript m refers to the measured value of the combined radiogenic and detrital components [28]. Secular equilibrium in ^{238}U–^{234}U–^{230}Th system is typically reached after ~400 kyr. While it is sometimes possible to date speleothems on million-year time scales using U–Pb (e.g., [31]), difficulty in accounting for initial ^{206}Pb has limited use of the technique thus far.

Drip-type speleothem growth is episodic. As a result, these speleothems can begin to accumulate in cave passages anytime after they are drained of groundwater [6–8]. In fact, climate change [26,32], rather than water table lowering, often initiates speleothem growth. Furthermore, sampling the oldest available speleothems is often difficult because speleothems tend to accumulate in certain heavily decorated areas where older deposits are covered by younger deposits. The best approach for obtaining speleothem ages that accurately date cave development is therefore to date several speleothems from each level, and use the oldest age for calculating an incision rate [8].

3.2. Sediment paleomagnetism

Paleomagnetism provides an important first-order assessment of the timing of fine sediment deposition in caves, provided magnetic reversals of known age can be identified in a stratigraphic sequence (e.g., [10,33–35]). Magnetic minerals become oriented to-

ward Earth's magnetic pole during deposition. Paleomagnetic dating involves correlating a local magnetostratigraphic column with the global paleomagnetic record. The chronology of magnetic reversals is well-established, with the last full reversal, the Matuyama–Brunhes, occurring ca. 0.78 Ma [36]. The presence of magnetically reversed sediments therefore indicates a minimum cave age of $\geq$0.78 Ma. Assuming constant sedimentation, paleomagnetism has been used to date caves back several million years (e.g., [33–35]).

As a dating tool, paleomagnetism suffers from two main limitations. First, it is a correlative tool that cannot yield absolute ages for stratigraphic units except when magnetic reversals are identified and reliably correlated with the global record. Cave sediment magnetostratigraphy therefore requires extensive sampling of a sedimentary sequence extending to the present time. If sedimentation is not constant, then reversals may not be recorded, leading to misidentification of chrons and erroneously young cave age estimates. Second, paleomagnetism is best recorded in fine sediments, the deposition of which may also significantly lag cave development. Paleomagnetism may also be applied to speleothems to extend the limit of U–Th dating (e.g., [26]), but the same limitations apply.

3.3. Cosmogenic burial dating

A recently developed method for dating buried sediment utilizes the concentration ratio of ^{26}Al and ^{10}Be [37,38]. These cosmogenic nuclides are produced in quartz within the top few meters of the earth's surface by secondary cosmic rays. Sediment accumulates ^{26}Al and ^{10}Be as it is exhumed from hillslopes and transported through river systems. Following Granger et al. [14], in a steadily eroding outcrop, the concentration (N_i) of either ^{26}Al or ^{10}Be in quartz at the surface is determined by Eq. (3):

$$N_i = \frac{P_n}{(1/\tau_i + \rho\varepsilon/\Lambda_n)} + \frac{P_\mu}{(1/\tau_i + \rho\varepsilon/\Lambda_\mu)} \quad (3)$$

where P_n is the production rate by nucleon spallation, P_μ is the production rate by muons, Λ_n is the exponential penetration length for nucleons ($\Lambda_n \approx 160$ g cm^{-2} [39]), Λ_μ is the exponential penetration length for muons ($\Lambda_\mu \approx 1300$ g cm^{-2} [40]), τ_{26} is the ^{26}Al radioactive meanlife ($\tau_{26}=1.02\pm0.04$ My [41]) and τ_{10} is the ^{10}Be radioactive meanlife ($\tau_{10}=2.18\pm0.09$ My [42, but see Section 5.3]). If sediment is then buried deeply enough (typically >20 m) that cosmic rays are shielded, nuclide production drastically slows or ceases and the products decay exponentially:

$$N_i = (N_i)e^{-t/\tau_i} \quad (4)$$

where t is the time since burial. Because ^{26}Al decays roughly twice as fast as ^{10}Be, the inherited nuclide ratio $(N_{26}/N_{10})_0$ decreases exponentially over time according to Eq. (5):

$$\frac{N_{26}}{N_{10}} = \left(\frac{N_{26}}{N_{10}}\right)_o e^{-(1/\tau_{26}-1/\tau_{10})} \quad (5)$$

where N_{26} and N_{10} are the concentrations of ^{26}Al and ^{10}Be, and $(N_{26}/N_{10})_0$ represents the inherited ^{26}Al/^{10}Be ratio as determined from Eq. (3). ^{26}Al/^{10}Be ratios in buried sediments may be used to determine burial ages from ~0.3 to 5.5 Ma [38,43]. Burial dating uses only quartz, a common mineral on the surface, and can provide absolute ages for coarse sediments without relying on correlation.

4. Field site

We dated cave deposits in the Sierra Nevada mountains of California (Fig. 2) using U–Th, paleomagnetism, and cosmogenic burial dating. The Sierra Nevada is well-suited for this study because caves are present at many elevations, and because caves contain abundant material suitable for all three dating methods. Although the majority of exposed bedrock in the Sierra Nevada is plutonic, highly fragmented metamorphic pendants containing thin marble septa are scattered across the range. Numerous caves have formed as surface streams encountered marble bedrock and diverted underground, forming caves as described above. Relatively rapid (up to 0.3 mm yr^{-1}) bedrock incision has preserved extensive multilevel caves in the steep canyon walls [15]. These caves present ideal settings to compare the accuracy of cave dating methods: accurately dated deposits from these caves should (1) show an older-upward age pattern for samples taken from tiered cave levels,

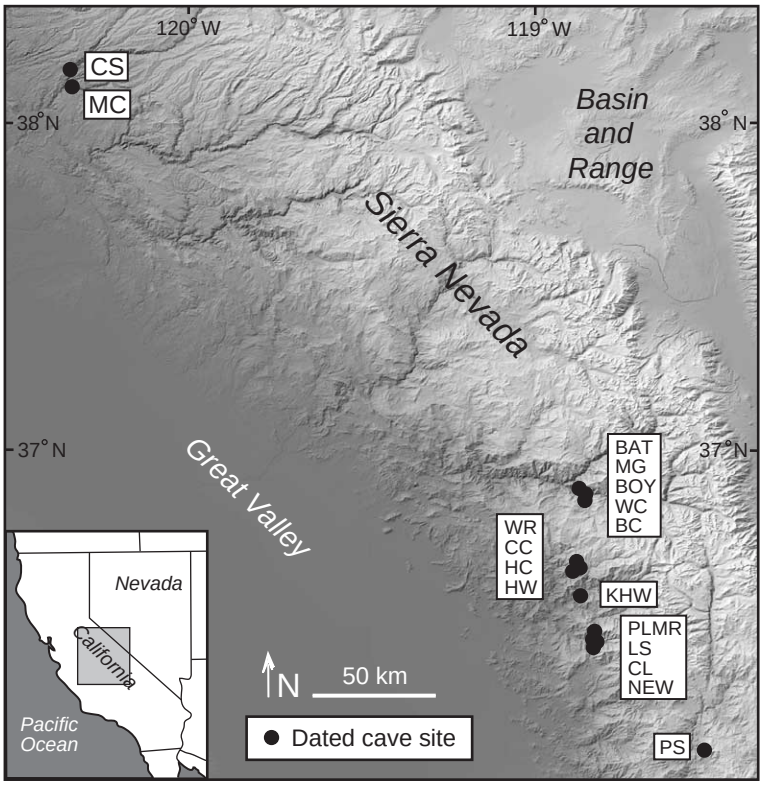

Fig. 2. Map of Sierra Nevada showing locations of sampled caves. See Tables 1 and 2 for key to cave names.

(2) show younger-upward age pattern for samples taken from a single sedimentary deposit, and (3) yield similar ages for samples collected from the same cave level.

5. Sampling, analytical methods, and results

5.1. U–Th speleothem dating

We collected 18 speleothem samples from seven caves for U–Th dating (see Appendix A for detailed sampling information). Approximately 1 g of calcite was cut from the cleanest basal layer of each sample, detrital grains removed by hand, and the remaining calcite dissolved in 8N HNO_3. Samples were measured by both thermal ionization mass spectrometry (TIMS) and inductively coupled plasma mass spectrometry (ICPMS). Samples measured by TIMS were spiked with ^{233}U and ^{229}Th, and U and Th coprecipitated with $Fe(OH)_3$ and purified by ion-exchange chromatography [44]. Purified U and Th were loaded onto single zone-refined Re filaments with colloidal graphite and run on a VG 54/WARP TIMS. Measured $^{234}U/^{235}U$ for SRM U010 was $0.00538 \pm 0.5\%$. Samples measured by ICPMS were initially prepared as above, except 25 μl aliquots of whole sample digests were spiked with ^{236}U and ^{229}Th and their concentrations measured by isotope dilution on a Thermo Finnigan Element ICPMS. U and Th were then purified as above, and isotopic ratios measured on a Thermo Finnigan Neptune multi-collector ICPMS by bracketing with UCSC standards and correcting for instrumental mass bias with National Institute of Standards and Technology (NIST) standards.

Speleothem ages from Sierra Nevada caves range from 21.9 ± 0.4 to ≥ 400 ka (Table 1). Of the 18 samples analyzed, only two were found to be in U–Th secular equilibrium (≥ 400 ka). Several samples contained significant initial ^{230}Th as indicated by relatively high ^{232}Th concentrations and low $^{230}Th/^{232}Th$ activity ratios (Table 1). We determined an R_0 value of

Table 1
Speleothem U-series ages for Sierra Nevada caves

Cave	Sample	Height (m)	U (ppb)	Th (ppb)	$\left[\frac{^{230}Th}{^{232}Th}\right]_{Act}$	$\left[\frac{^{234}U}{^{238}U}\right]_{Act}$	$\left[\frac{^{230}Th}{^{234}U}\right]_{Act}$	Uncorrected age[b] (ka)	Corrected age[c] (ka)
Crystal Stanislaus Cave[a]	CS-1U	98 ± 5	55.8	12.8	12	1.093	0.788	158.4 ± 3.1	151.7 ± 3.8
Crystal Stanislaus Cave	CS-2U	98 ± 5	29.8	1.3	55	1.065	0.755	133.1 ± 2.6	131.7 ± 3.3
Crystal Stanislaus Cave	CS-3U	95 ± 5	28.6	0.5	113	1.069	0.616	93.2 ± 1.8	92.7 ± 2.3
McLeans Cave[a]	MC-1U	30 ± 2	43.3	11.4	6	1.081	0.378	51.3 ± 1.9	44.0 ± 2.8
McLeans Cave[a]	MC-2U	28 ± 2	72.5	1.7	75	1.043	0.578	88.2 ± 1.2	87.5 ± 1.4
Windy Cliff Cave[a]	WC-1U	19.5 ± 1	582.7	140.6	4	1.134	0.254	27.5 ± 3.1	26.4 ± 3.5
Crystal Cave (Bear Den Cave)	CC-BD-1U	62 ± 1	218.7	6.8	81	1.019	0.811	173.4 ± 3.4	172.5 ± 4.3
Crystal Cave (Bear Den Cave)	CC-BD-2U	59 ± 1	103.5	0.2	304	1.027	0.208	25.6 ± 0.5	25.4 ± 0.6
Crystal Cave (Phosphorescent Room)[a]	CC-PR-1U	36.5 ± 1	438.2	144.7	3	0.962	0.285	36.1 ± 0.3	24.7 ± 0.8
Crystal Cave (Organ Balcony)[a]	CC-OB-1U	28 ± 1	280.7	5.5	30	1.031	0.182	21.9 ± 0.4	21.3 ± 0.6
Crystal Cave (Marble Hall)	CC-MH-1U	14 ± 1	76.5	7.2	41	1.017	1.203	≥400	≥400
Crystal Cave (Curtain Room)	CC-CR-1U	12.5 ± 1	76.7	2.7	18	1.070	0.198	22.4 ± 0.4	21.3 ± 0.7
Weis Raum Cave[a]	WR-1U	212 ± 2	49.4	65.8	16	1.027	0.6719	121.2 ± 3.0	116.3 ± 3.7
Headwall Crawl Cave	HW-1U	37.5 ± 1	94.4	17.9	8	0.990	0.478	72.4 ± 1.4	65.8 ± 1.6
Soldiers Cave (Waiting Room)	LS-WR-2U	43 ± 2	153.3	62.2	4	1.144	0.490	60.6 ± 1.2	49.0 ± 1.3
Soldiers Cave (Aragon Room)	LS-AR-1U	43 ± 2	70.0	5.7	7	1.148	0.123	17.2 ± 0.4	14.7 ± 0.7
Soldiers Cave (Ruby's Route)	LS-RR-1U	41 ± 2	254.1	14.2	40	1.067	0.709	118.3 ± 2.4	116.5 ± 2.9
Packsaddle Cave	PS-1U	45 ± 5	178.4	21.6	35	0.995	1.378	≥400	≥400

[a] Isotopic ratios for these samples determined by thermal ionization mass spectrometery (TIMS), all others determined by multi-collector ICP-MS. [b] Ages determined by solution of Eq. (1), where $\lambda_{230}=9.1577\times10^{-6}$ yr^{-1} and $\lambda_{234}=2.8263\times10^{-6}$ yr^{-1} [30]. Uncertainties are 2σ and include analytical and systematic uncertainties. [c] Ages corrected for initial ^{230}Th using Eq. (2), assuming an initial $[^{230}Th/^{232}Th]_{Act}$ value of 0.98 for the detritus and secular equilibrium in the U-series.

0.98 for the detrital component of one highly contaminated sample (WC-1U) by total dissolution isochron methods [30], and used this value, assumed to characterize the regional R_0 value, to correct ages using Eq. (2) (Table 1). Although correcting for detrital ^{230}Th by this method increases total age uncertainty, we will show that the magnitude of error associated with this correction is small when compared to the age disparities between different dating methods.

5.2. Sediment paleomagnetism

We collected 44 fine sediment samples from five caves for paleomagnetic analyses (see Appendix A for detailed sampling information). Samples were analyzed in plastic cubes in a 3-axis 2-G superconducting rock magnetometer. All samples underwent stepwise alternating field (AF) demagnetization in 4–10 steps ranging between 0 (natural remanent magnetism, or NRM) and 120 mT, until 90% of their initial NRM strength was removed. Orthogonal vector plots [45] provided points for principal component analysis to extract characteristic remanent magnetic vectors [46]. Lower-coercivity demagnetization directions were visually removed from high-coercivity directions; mean directions for high-coercivity components were determined using Fisher [47] statistics.

Paleomagnetic samples generally showed very well-behaved demagnetization paths, in which application of a 10 mT peak AF removed a low-coercivity viscous normal overprint (Fig. 3A). Clean demagnetization paths that converge on the origin and loss of over 95% of the sample field strength during AF demagnetization at 100–120 mT conclusively support the interpretation of the majority of samples as normal. If a "hidden" reverse field component were present (as we have seen in samples from caves in other areas), we would expect non-convergence on the origin and a "hooked" path (Fig. 3A). Vector averaging [47] results in a mean paleomagnetic direction for normal samples of inclination 49.3° and declination 356.8°, with a α_{95} of 5.53°; this direction is close to the calculated axially centered dipole for the southern Sierra Nevada (Fig. 3B).

Thirty-eight of the 44 samples exhibit a distinct normal polarity signal, while two samples exhibit

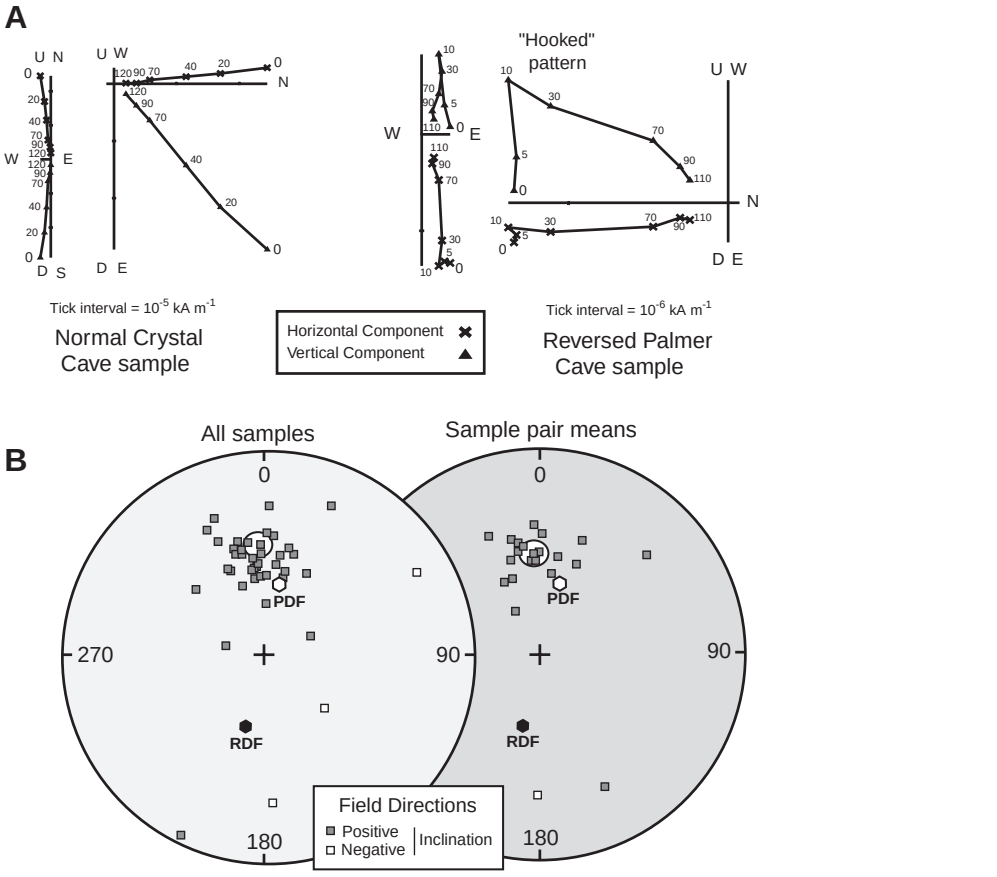

Fig. 3. Paleomagnetic results. A: Representative orthogonal vector plots of normal and reverse samples. Left panel shows straightforward normal polarity, right panel shows viscous remnant magnetization removed by alternating field demagnetization; underlying reverse polarity vector decays toward origin in "hooked" pattern. B: Stereographic projections of paleomagnetic field directions for all samples (left) and sample pair means (right). White ellipse shows α_{95} confidence limits. Present day field (PDF) and equivalent reverse direction field (RDF) shown as white and black hexagons, respectively.

normal polarity with high-to-moderate certainty. Only four samples show a reverse polarity signal. These samples were collected from Palmer Cave, the highest cave above modern river level. While these reversed sediments demonstrate that Palmer Cave is older than ~780 kyr [36], they cannot be correlated to a particular reversed period due to lack of a continuous stratigraphic section extending to the present.

5.3. Cosmogenic burial dating

We collected 26 deeply buried coarse sediment samples from 13 caves for burial dating (see Appendix A for detailed sampling information). Samples were crushed and sieved to 0.25–0.5 mm, and ~80–100 g of quartz purified from each sample by selective chemical dissolution [48]. Samples were spiked with ~0.4 mg ^{9}Be in a low blank (^{10}Be/^{9}Be$=3.0\pm0.3\times10^{-15}$) Be carrier prepared from deep mined beryl [49]. Quartz was dissolved in concentrated HF and HNO_3, fluorides expelled with $HClO_4$ fuming, and Al and Be separated and purified by ion-exchange chromatography and selective precipitation. Hydroxide precipitates were oxidized, mixed with Ag (for Al) and Nb (for Be) powders, and packed into stainless steel or aluminum targets, respectively. ^{10}Be/^{9}Be and ^{26}Al/^{27}Al ratios were determined by accelerator mass spectrometry (AMS) at Lawrence Livermore

National Laboratory (LLNL) and normalized to ICN ^{10}Be and NIST ^{26}Al standards. Mean process blanks were generally low (^{26}Al/^{27}Al=2.0±4.0×10^{-15}, ^{10}Be/^{9}Be=4.0±0.3×10^{-15}) compared to samples. Stable Al concentrations were determined by ICP optical emission spectrometry and assigned 4% error. Repeat ^{26}Al/^{27}Al measurements show very good reproducibility (Table 3).

Cave sediments yielded burial ages ranging from 0.30±0.10 to ≥4.72 Ma (Table 2). This represents the effective bounds of the burial dating technique; decay of ^{26}Al to extremely low concentrations limits the age of the oldest sample to ≥4.72 Ma. We normalized ^{10}Be/^{9}Be measurements to LLNL ^{10}Be secondary standards calibrated against an ICN standard with a ^{10}Be meanlife of 2.18±0.09 My [42]. Some researchers (e.g., [17]) favor a standard prepared by NIST with a ^{10}Be meanlife of 1.93±0.10 My [42], ~14% lower than that based on the ICN standard. Using the NIST meanlife lowers measured ^{10}Be/^{9}Be ratios by 14%, lowers the ^{10}Be production rate by the same amount, and increases burial ages non-linearly. Until the meanlife ambiguity is resolved, we use the commonly accepted value of 2.18±0.09 My, but report alternative burial ages based on the NIST standard meanlife (Table 2). Using the alternative meanlife does not affect the conclusions we draw here.

Burial age accuracy hinges on the assumption that sediment did not experience prior burial before entering caves, which would diminish ^{26}Al/^{10}Be production ratios and yield erroneously old ages (e.g., [50]). Although we cannot completely exclude the possibility of prior burial, we consider this unlikely in the Sierra Nevada. In order to measurably diminish ^{26}Al/^{10}Be ratios, sediment must be buried for >100 kyr at large depths (>5 m), or even longer at shallower depths [38]. There are virtually no river terraces in the narrow canyons upstream of sampled caves, and steep

Table 2
Cosmogenic nuclide concentrations and sediment burial ages for Sierra Nevada caves

Cave	Sample	Height (m)	^{26}Al (10^4 atm g^{-1})	^{10}Be (10^4 atm g^{-1})	^{26}Al/^{10}Be	Burial age[a] (Ma)	NIST burial age[b] (Ma)
Crystal Stanislaus Cave	CS-1	92±5	26.56±0.98	10.28±0.21	2.59±0.11	1.63±0.08 (0.16)	1.81±0.09 (0.22)
Morning Glory Cave	MG-1	274±5	25.03±1.55	13.30±0.33	1.88±0.13	2.34±0.19 (0.30)	2.58±0.19 (0.39)
Bat Cave	BAT	395±5	11.15±0.93	6.64±0.16	1.48±0.16	2.70±0.21 (0.38)	2.90±0.21 (0.49)
Boyden Cave	BOY-2	42.5±1	36.41±1.36	12.43±0.30	2.93±0.13	1.38±0.08 (0.15)	1.54±0.09 (0.21)
Bear Cave	BC-1	8±1	56.24±2.61	10.92±0.28	5.15±0.22	0.32±0.10 (0.18)	0.33±0.11 (0.25)
Weis Raum Cave	WR-1	212±2	9.46±0.75	5.50±0.12	1.72±0.14	2.42±0.16 (0.28)	2.69±0.16 (0.36)
Hurricane Crawl Cave	HC-PL-1	39.5±1	35.23±1.93	9.44±0.24	3.73±0.23	0.93±0.12 (0.24)	1.02±0.12 (0.31)
Crystal Cave (Bear Den Cave)	CC-BD	58±1	97.53±4.10	29.81±0.70	3.27±0.16	1.15±0.09 (0.16)	1.28±0.10 (0.22)
Crystal Cave (Phosphorescent Room)	CC-PR	36.5±1	311.90±8.7	91.80±2.6	3.39±0.14	1.00±0.07 (0.15)	1.14±0.08 (0.20)
Crystal Cave (Fat Man's Misery)	CC-FM-1	22.5±1	79.17±3.41	20.47±0.49	3.87±0.19	0.86±0.09 (0.16)	0.93±0.10 (0.21)
Crystal Cave (Junction Room)	CC-LR-1	8.5±1	107.20±3.5	23.79±0.56	4.51±0.18	0.56±0.08 (0.15)	0.60±0.08 (0.19)
Kaweah Cave	KHW-1	17±1	7.36±0.78	1.49±0.25	4.94±0.99	0.40±0.38 (0.45)	0.42±0.38 (0.59)
Palmer Cave	PLMR-1	685±5	≤1.21	2.34±0.14	≤0.52	≥4.72	≥5.29
Clough Cave	CL-1	53.5±2	7.33±0.61	2.09±0.07	3.51± 0.31	1.03±0.13 (0.24)	1.09±0.14 (0.33)
New Cave	NEW-1	34±2	54.44±2.44	13.85±0.33	3.93±0.20	0.83±0.10 (0.18)	0.90±0.10 (0.23)
Soldiers Cave (Entrance Room)	LS-RH-1	83±2	50.24±3.24	15.94±0.38	3.15±0.22	1.25±0.13 (0.20)	1.37±0.13 (0.26)
Soldiers Cave (Waiting Room)	LS-WR-1	41±2	71.36±2.97	19.63±0.49	3.64±0.18	0.98±0.09 (0.17)	1.06±0.10 (0.23)
Soldiers Cave (Corridor)	LS-LC-1	12.5±2	73.93±3.21	15.03±0.36	4.92±0.24	0.40±0.09 (0.17)	0.42±0.10 (0.22)
Modern river sediment	KGR-1	0±0	22.68±1.17	3.61±0.07	6.26±0.35	−0.06±0.11 (0.21)	−0.06±0.11 (0.26)
Modern river sediment	KWH-1	0±0	35.25±1.65	5.90±0.16	5.97±0.32	0.04±0.10 (0.18)	0.04±0.10 (0.22)

[a] Burial ages determined by iterative solution of Eqs. (3) (4) (5), assuming sea level high latitude (SLHL) neutron production rates of P_{26}=31.1 atm g^{-1} yr^{-1} and P_{10}=5.1 atm g^{-1} yr^{-1} [53], and SLHL stopped muogenic production rates of P_{26}=0.80 atm g^{-1} yr^{-1} and P_{10}=0.10 atm g^{-1} yr^{-1} [54]. Uncertainties represent 1σ measurement uncertainty. Systematic uncertainties in production rates (20%), ^{26}Al/^{10}Be production ratio [53] and radioactive decay constants [41,42] are added in quadrature and shown as total uncertainty in parentheses. When comparing burial ages, analytical uncertainties are used; when comparing burial ages with other dating methods, total uncertainties are used.
[b] Alternative burial ages calculated using a ^{10}Be meanlife of 1.93±0.10 Ma and the National Institute of Standards and Technology (NIST) Be standard [42].

Table 3
Cosmogenic $^{26}Al/^{10}Be$ burial age reproducibility

Cave	Sample	^{26}Al conc. (10^4 atm g^{-1})	Mean ^{26}Al conc. (10^4 atm g^{-1})	^{10}Be conc. (10^4 atm g^{-1})	$^{26}Al/^{10}Be$	Burial age (Ma)[b]
Bat Cave	BAT-1	11.15 ± 0.93	–	6.65 ± 0.16	1.68 ± 0.15	2.45 ± 0.16
	BAT-2	12.33 ± 3.61	–	6.74 ± 0.17	1.83 ± 0.54	2.28 ± 0.49
	BAT-3A	10.22 ± 1.45	11.30 ± 0.97	7.52 ± 0.56	1.50 ± 0.17	2.70 ± 0.21
	BAT-3B[a]	12.19 ± 1.31				
	BAT-4A	10.42 ± 1.67	10.23 ± 0.90	6.64 ± 0.16	1.54 ± 0.14	2.61 ± 0.17
	BAT-4B[a]	10.15 ± 1.07				
Boyden Cave	BOY-1	56.09 ± 2.08	–	11.41 ± 0.28	4.92 ± 0.22	0.39 ± 0.08
	BOY 2	36.41 ± 1.36	–	12.43 ± 0.30	2.93 ± 0.13	1.38 ± 0.08
Crystal Cave (Bear Den Cave)	CCBD-1	97.53 ± 4.10	–	29.81 ± 0.69	3.27 ± 0.16	1.16 ± 0.09
	CCBD-2	54.72 ± 2.11	–	16.51 ± 0.40	3.31 ± 0.15	1.14 ± 0.09
Crystal Cave (Phosph. Room)	CCPR-1	311.89 ± 8.77	–	91.94 ± 2.60	3.39 ± 0.14	1.06 ± 0.07
	CCPR-2	262.44 ± 8.21	–	72.49 ± 1.67	3.62 ± 0.14	0.94 ± 0.07
Clough	CL-2A	7.56 ± 0.91				
	CL-2B[a]	6.72 ± 0.80	7.38 ± 0.48	2.09 ± 0.06	3.53 ± 0.25	1.03 ± 0.13
	CL-2C[a]	7.88 ± 0.78				

[a] Indicates samples with replicate $^{26}Al/^{27}Al$ measurement only. Resulting $^{26}Al/^{10}Be$ ratios and burial ages utilize replicate $^{26}Al/^{27}Al$ measurements, but only one $^{10}Be/^{9}Be$ measurement. [b] Total uncertainties (in parentheses in Table 2) are not reported because the factors leading to these uncertainties affect all burial ages equally and are not relevant when comparing burial ages.

channel gradients imply rapid sediment transport. Although glaciated headwater regions of the larger river systems do contain moraine and outwash deposits that could store deeply buried sediment, it is unlikely that such deposits stored sediment for long enough to significantly alter $^{26}Al/^{10}Be$ ratios because frequent glaciations scoured out these canyons on ≤100 kyr time scales. Lack of an inherited burial signal in Sierra Nevada sediment is demonstrated by numerous cosmogenic nuclide measurements [51,52], including our own from modern river systems (Table 2), which show $^{26}Al/^{10}Be$ ratios within error of the expected surface production ratio of 6.1 [53].

Unlike speleothem ages, which may be expected to vary within a single cave level, coarse sediment burial ages should be similar, testing both burial age accuracy and our cave development model. We replicated burial ages from four cave levels, and generally found very good agreement of ages, well within analytical errors (Tables 3 and 4). In only one case do sediment burial ages disagree substantially. Two samples from Boyden Cave yield burial ages of 0.39 ± 0.08 Ma and 1.38 ± 0.08 Ma, a discrepancy well outside analytical uncertainty (Tables 3 and 4). We suspect that the younger sample is anomalous because it was collected near a seasonal underfit stream that apparently entered the cave recently and was not instrumental in its formation; this stream may have carried sediment into the cave well after it formed. In contrast, the older sample was collected from a ledge 3 m above the floor and more likely represents sediment emplaced during the original development of the

Table 4
Statistics of cosmogenic $^{26}Al/^{10}Be$ burial age reproducibility

Cave	Sample	Weighted average age (Ma)[a]	Standard deviation (Ma)	Weighted analytical uncertainty (Ma)	Reduced χ^2	Probability[b]
Bat	BAT	2.55 (n=4)	0.12	0.10	0.36	0.78
Boyden	BOY	0.89 (n=2)	0.70	0.06	70	10^{-16}
Bear Den	CCBD	1.15 (n=2)	0.01	0.06	0.02	0.89
Crystal	CCPR	1.00 (n=2)	0.08	0.05	1.21	0.27

[a] Weighted by inverse variance normalized by average inverse variance. [b] Probability that analytical uncertainty accounts for all observed variance.

passage. The discrepancy illustrates a level of complexity of cave development not shown in Fig. 1, highlighting the importance of careful sample selection and interpretation.

6. Discussion

6.1. Comparison of dating methods

The three dating methods employed in this study all provide minimum cave ages that yield maximum rates of incision. However, comparison of ages suggests that U–Th dating of speleothems and paleomagnetism of fine sediment are prone to underestimating cave age, leading to overestimates of incision rates.

Recall that cave ages increase with height above modern rivers; dated deposits should display this older-upward pattern if they accurately date cave development. Sierra Nevada speleothem ages generally increase in age with height above modern rivers, but the trend is complicated by two samples with ages ≥400 ka (Fig. 4). These two speleothems sit relatively close to modern river levels; in both cases, speleothems from stratigraphically higher positions yielded younger ages (Fig. 4). The required older-upward pattern effectively

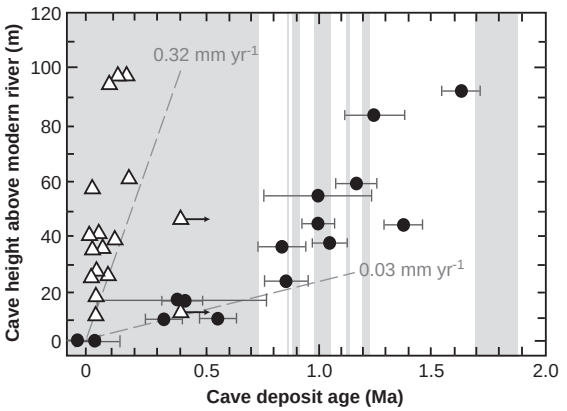

Fig. 4. Speleothem U–Th (white triangles) and sediment burial (black circles) ages for all cave passages up to 100 m above modern river levels. Speleothem ages are much younger than sediment burial ages from similar cave heights. Gray dashed lines depict hypothetical maximum incision rates based on speleothem age-elevation distributions (see text for discussion). Error bars represent 1σ uncertainty; where not visible, error bars are smaller than marker symbol. For reference, normal polarity chrons are shown in gray, reversed polarity in white [36].

negates the stratigraphically higher speleothem ages, as they cannot be younger than those below and still represent plausible cave ages. Furthermore, basal speleothem samples collected from the same cave levels show considerable age variations (Fig. 4, Table 1). Stratigraphic inconsistency and variable ages from similar heights suggest that speleothem ages often do not accurately date cave development.

The most striking aspect of the speleothem ages is how much they differ from sediment burial ages collected from similar heights (Fig. 4). Coarse sediments are much older than speleothems at virtually every site studied (Fig. 4). Burial ages from all but the lowest (<20 m height) cave levels are much greater than 400 ka, the approximate limit of U–Th dating. Thus, except in the very lowest levels, speleothem U–Th ages are not capable of capturing cave ages as indicated by burial dating. The ~400 ka limit of U–Th alone presents a serious limitation of speleothems to accurately date cave development. Yet more troubling, perhaps, is that most speleothem ages are in fact much younger than the 400 ka limit (Table 1; Fig. 4). This is similar to patterns shown by compilations of speleothem age distributions (e.g., [26,27]) suggesting climatic controls on speleothem growth. The result is that, rather than simply recording ages of ≥400 ka for very old cave passages, speleothems may record "absolute" ages that are much younger, yielding misleadingly fast incision rates. Note that the offset between speleothem and sediment ages cannot be due to uncertainty in age corrections, as correction for initial ^{230}Th and use of the alternative ^{10}Be meanlife both tend to increase this offset.

The paleomagnetic results are somewhat more difficult to interpret. No reversed sediments were found in passages lower than 100 m height, despite burial ages spanning the past 1.6 Myr (Fig. 4). We can think of five reasons why reversed sediments were not found in these passages: 1) many samples are in fact reversed, but a viscous normal overprint was not removed by AF demagnetization, 2) the cosmogenic ^{26}Al/^{10}Be burial ages are erroneously old because of prior sediment burial, 3) reversed sediments are present but were not sampled, 4) fine-grained sedimentation occurred in pulses coincident with short normal polarity chrons, or 5) much of the fine sediment has been deposited or remobilized since the last magnetic reversal. We have already presented arguments against the first two rea-

sons. The remaining three hypotheses are plausible. Burial ages suggest that more than half of the sampled coarse sediment deposits entered caves during the reversed Matuyama chron (Fig. 4). Although there are considerable spatial gaps in our paleomagnetic sampling, we consider it unlikely that we simply missed sampling a reversal. In all cases but one, uncertainties in the burial ages do allow for deposition of fine-grained sediment nearly synchronously with coarse sediment during many of the short normal chrons that occurred within the Matuyama chron (Fig. 4). However, this explanation requires an uncomfortable degree of coincidence. We consider the last explanation to be the most likely: that final deposition of fine sediment lagged deposition of coarse sediment, potentially by tens to hundreds of thousands of years, due to remobilization and deposition during flood events that can waft sediment high into upper level passages (Fig. 1). Such floods are not unexpected in the mountainous Sierra Nevada, where even historical floods have increased mean peak river discharges by orders of magnitude. Discordance between coarse sediment burial ages and fine sediment paleomagnetism has been noted in other flood-prone caves [14].

We argue that the discrepancies in cave ages shown by the three dating methods are best explained in terms of the timing of deposition. In most cases, only coarse sediment can be reasonably assumed to have been deposited during the waning stages of cave development. Fine sediment is easily reworked, and can be deposited much later by floods entering cave passages well above base level. Inception of drip-type speleothem growth does not relate to base level lowering, and may commence at any time. The age discrepancies shown by the three dating methods suggest potentially large time lags between deposition of these materials, even when they are in close proximity.

6.2. Direct comparison of dating methods: Crystal Cave

Thus far we have compared all of the dated cave deposits rather broadly using the model of cave development outlined in Fig. 1. How well do adjacent deposits in the same cave, and even in the same sediment deposit, compare? We collected 30 sediment and speleothem samples from Crystal Cave (Fig. 5), a multilevel cave with abundant stratified deposits (see Appendix A). The development of Crystal Cave closely mirrors the conceptual model illustrated in Fig. 1: as bedrock incision of Cascade Creek lowered the water table through time, multiple cave levels were left perched progressively higher within a steep ridge (Fig. 5A).

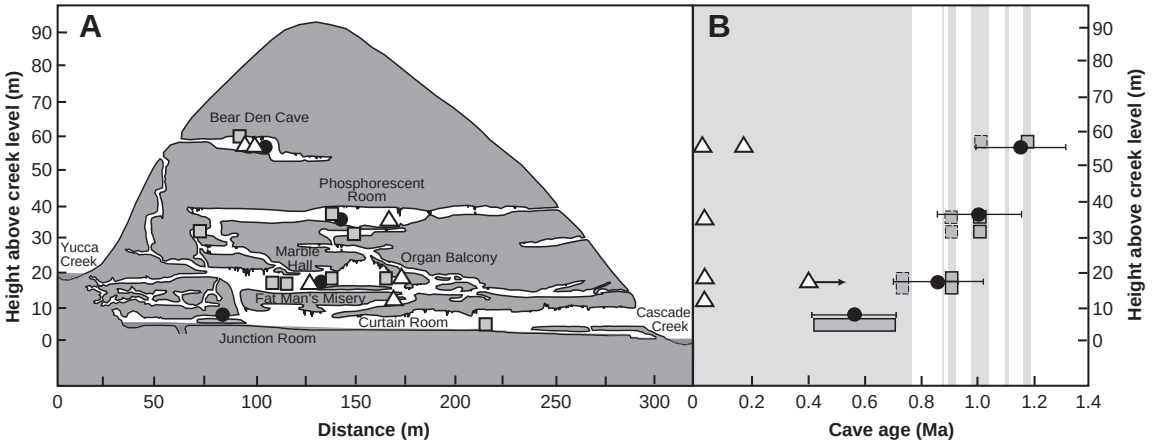

Fig. 5. A. Profile map of Crystal Cave showing speleothem U–Th (white triangles), paleomagnetic (gray squares), and cosmogenic burial (black circles) samples. B. Deposit ages as a function of height above Cascade Creek. Offset between speleothem U–Th ages and sediment burial ages from similar heights reveals time lag between deposition of coarse sediment and overlying speleothems. For reference, normal polarity chrons are shown in gray, reversed polarity in white [36]. All paleomagnetic samples are normal and must be correlated with deposition during normal chron(s); correlations assuming deposition coincident with coarse sediment are shown as gray squares, but deposition of all fine-grained sediment after 0.78 Ma is also possible.

The ages from Crystal Cave mirror the age disparities found in other caves. Speleothem ages range from 21.9 ± 0.4 to ≥ 400 ka, but do not show a clear trend of increasing age with height above Cascade Creek (Fig. 5). A ≥ 400 ka aged speleothem (CC-MH-1U) is the second lowest sample, indicating that none of the stratigraphically higher speleothems provide accurate cave ages. In contrast, sediment burial ages range from $0.56 \pm (0.16)$ to $1.17 \pm (0.18)$ Ma and show the expected older-upward pattern (Fig. 5B). Multiple burial samples collected from two levels show excellent age agreement, well within analytical uncertainty (Tables 3 and 4). Although the ≥ 400 ka age of CCMH-1U may at first seem anomalous, and therefore suspect, when compared with other speleothem ages, burial ages suggests that this is the only dated speleothem that correctly identifies the passage age.

Interstratified calcite and sediments offer the most direct comparison of dating methods, but such deposits are rare in Sierra Nevada caves, and are generally uncommon. In the one instance in which we found interstratified calcite, it was too contaminated with detrital Th to obtain a reliable U–Th age, a frequent problem with dating such layers. However, we were able to apply all three dating methods to one stratified deposit in Crystal Cave (Fig. 6). Burial dating of coarse sand and gravel resting on bedrock yielded an age of $860 \pm (160)$ ka. An overlying silt layer shows a clear normal polarity signal. In this case, the burial age and magnetic polarity are generally consistent. If the silt was deposited shortly after the coarse sediment (for instance, during the waning slack water stage of a flood event), then the normal polarity serves to reduce the uncertainty in the burial age, suggesting that the coarse sediment was deposited just prior to the last magnetic field reversal 780 ka. The capping speleothem layer yielded an age of ≥ 400 ka, consistent with both the burial age and the paleomagnetic orientation, but obviously not providing precise age control. If only the minimum age of 400 ka were used to estimate the age of this passage, it would underestimate the age by at least a factor of two. In other passages, age discrepancies between coarse sediment and adjacent speleothems are greater than an order of magnitude (Fig 5B).

7. Implications for landscape evolution studies

Speleothem U–Th ages provided the first quantitative estimates of landscape evolution based on cave development (e.g., [7,24–26]), and continue to be

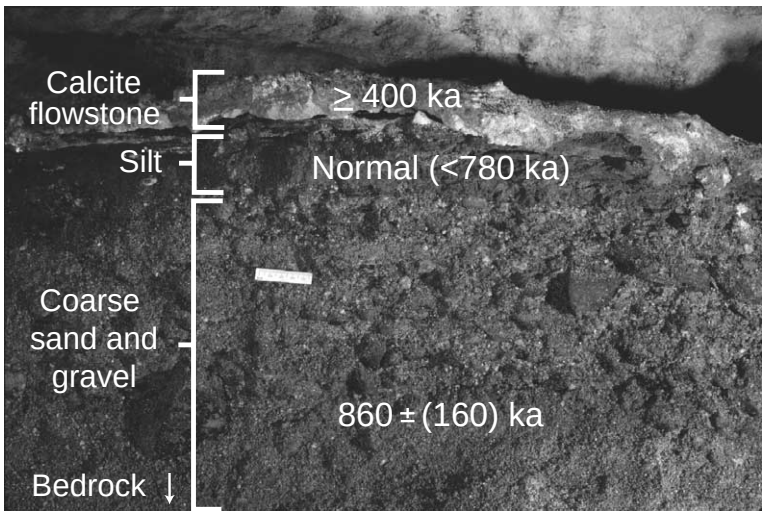

Fig. 6. Stratified deposit ages from Crystal Cave. Scale bar is 5 cm. Bedrock floor is just below bottom of photograph. Coarse sediment has a burial age of $860 \pm (160)$ ka. Overlying silt layer shows normal polarity, indicating deposition following Brunhes–Matuyama reversal 780 ka. Flowstone layer with a U–Th age of ≥ 400 ka caps deposit. Although deposit ages are stratigraphically consistent, only coarse sediment burial age provides accurate absolute age for cave passage development.

used in incision studies (e.g., [9]). These studies are usually explicit regarding the problem of minimum speleothem ages, and emphasize that resulting incision rates should be considered maximum rates. Unfortunately, the importance of these rates as maxima tends to become lost in subsequent citations, creating a bias toward fast rates of landscape evolution.

Until now the sensitivity of speleothem ages to potential bias in cave age, and thus in incision rate, has not been well-quantified. This sensitivity is clearly illustrated in Fig. 4. The steepest straight line drawn to include all speleothem ages yields a maximum incision rate of 0.03 mm yr^{-1} (Fig. 4). This line hinges on a single $\geq$400 ka age sample positioned relatively close to river level. If the two $\geq$400 ka age samples had not been collected, or if they were ignored as outliers, the inferred maximum incision rate based on the majority of speleothem ages would be 0.32 mm yr^{-1} (Fig. 4). Stated as a maximum, this latter rate is not incorrect, but it places only a basic constraint. In contrast, coarse sediment burial ages reduce maximum incision rates to ~0.03–0.05 mm yr^{-1}, and omitting any one data point does not significantly alter the slope of the maximum incision line (Fig. 4). Because coarse sediment deposition corresponds closely in time with cave development, burial ages provide more accurate estimates of cave age; they still provide only maximum incision rates, but these are likely much closer to the actual rates.

8. Conclusions

All cave deposits necessarily postdate cave development, and even the youngest deposits provide minimum cave ages that place maximum limits on landscape evolution rates. Yet, our results from Sierra Nevada caves suggest that relying on either drip-type speleothem U–Th ages or fine sediment paleomagnetism can greatly exacerbate the minimum age bias, promoting erroneously fast rates of landscape evolution. Speleothem U–Th ages, while accurately dating the inception of speleothem growth, provide the least accurate cave ages because speleothem growth often significantly lags cave development, and because U–Th dating is limited to ~400 ka. Paleomagnetism can place important age constraints on sediment deposition more likely contemporaneous with cave development, but is limited by the fact that caves frequently do not possess the continuous stratigraphic sections necessary to correctly correlate reversals, and by the fact that fine sediment can be remobilized and deposited by floods in passages well above base level. Episodic deposition can lead to misidentification of reversals, resulting in underestimation of cave ages and overestimation of incision rates. One of the key strengths of cosmogenic burial dating is that it requires no correlation with another time scale. Burial dating of coarse sediment further reduces minimum age bias because coarse sediment is usually deposited as bedload at or near base level during the waning stages of cave development. $^{26}Al/^{10}Be$ burial dating is particularly useful because it requires only quartz, a common clastic mineral, and because its age range, ~0.3–5 Ma, is well beyond the limit of U–Th dating.

Although simple stratigraphic relations dictate that speleothems be younger than underlying coarse sediment, our results reveal that speleothems may be younger by more than an order of magnitude. Fine sediment deposition is often younger than coarse sediment by an undeterminable amount. This suggests caution in using speleothem U–Th dating or fine sediment paleomagnetism alone to date caves for landscape evolution studies. When dating method limitations, stratigraphic relations, and complex depositional histories are considered, cosmogenic burial dating of coarse clastic sediment appears to be the best method for dating cave development in mountainous regions.

Acknowledgments

We thank Sequoia and Kings Canyon National Parks and Sequoia National Forest for permission to collect samples, and Joel Despain and Steve Bumgardner for help in the field. We gratefully acknowledge mass spectrometry assistance from Jugdeep Aggarwal, Daniel Sampson, and Rob Franks. Comments by Victor Polyak and three anonymous reviewers improved the manuscript. This research was funded by grants from the National Science Foundation (EAR-0126253), the Institute of Geophysics and Planetary Physics, and the Cave Conservancy Foundation. Cosmogenic nuclide measurements were

performed under the auspices of the U.S. Department of Energy by the University of California, Lawrence Livermore National Laboratory under contract W-7405-Eng-48.

Appendix A. Supplementary data

Supplementary data associated with this article can be found, in the online version, at doi:10.1016/j.epsl.2005.04.024.

References

[1] D.W. Burbank, J. Leland, E. Fielding, R.S. Anderson, N. Brozovic, M.R. Reid, C. Duncan, Bedrock incision, rock uplift, and threshold hillslopes in the northwestern Himalayas, Nature 379 (1996) 505–510.

[2] G.S. Hancock, R.S. Anderson, O.A. Chadwick, R.C. Finkel, Dating fluvial terraces with ^{10}Be and ^{26}Al profiles: application to the Wind River, Wyoming, Geomorphology 27 (1999) 41–60.

[3] W.D. Sharp, K.R. Ludwig, O.A. Chadwick, R. Amundson, L.L. Glaser, Dating fluvial terraces by ^{230}Th/U on pedogenic carbonate, Wind River Basin, Wyoming, Quat. Res. 59 (2003) 139–150.

[4] J. Wakabayashi, T.L. Sawyer, Stream incision, tectonics, uplift, and evolution of topography of the Sierra Nevada, California, J. Geol. 109 (2001) 539–562.

[5] D.W. Burbank, R.S. Anderson, Tectonic Geomorphology, Blackwell Science, 2001, 274 p.

[6] D.C. Ford, P.W. Williams, Karst Geomorphology and Hydrology, Unwin Hyman, London, 1989, 601 p.

[7] D.C. Ford, H.P. Schwarcz, J.J. Drake, M. Gascoyne, R.S. Harmon, A.G. Latham, Estimates of the age of the existing relief within the southern Rocky Mountains of Canada, Artic. Alpine Res. 13 (1981) 1–10.

[8] T.C. Atkinson, P.J. Rowe, Applications of dating to denudation chronology and landscape evolution, in: M. Ivanovich, R.S. Harmon (Eds.), Uranium-series Disequilibrium: Applications to Earth, Marine and Environmental Sciences, Oxford Univ. Press, Oxford, 1992, pp. 669–703.

[9] W. Fei, L. Hongchun, Z. Rixiang, Q. Feizhou, Late quaternary downcutting rates of the Qianyou River from U/Th speleothem dates, Qinling mountains, China, Quat. Res. 62 (2004) 194–200.

[10] I.D. Sasowsky, W.B. White, V.A. Schmidt, Determination of stream-incision rate in the Appalachian plateaus by using cave-sediment magnetostratigraphy, Geology 23 (1995) 415–418.

[11] A.R. Farrant, P.L. Smart, F.F. Whitaker, D.H. Tarling, Long-term Quaternary uplift rates inferred from limestone caves in Sarawak, Malaysia, Geology 23 (1995) 357–360.

[12] G.S. Springer, J.S. Kite, V.A. Schmidt, Cave sedimentation, genesis, and erosional history in the Cheat River canyon, West Virginia, Geol. Soc. Am. Bull. 109 (1997) 524–532.

[13] D.E. Granger, J.W. Kirchner, R.C. Finkel, Quaternary downcutting rate of the New River, Virginia, measured from differential decay of cosmogenic ^{26}Al and ^{10}Be in cave-deposited alluvium, Geology 25 (1997) 107–110.

[14] D.E. Granger, D. Fabel, A.N. Palmer, Pliocene–Pleistocene incision of the Green River, Kentucky, determined from radioactive decay of cosmogenic ^{26}Al and ^{10}Be in Mammoth Cave sediments, Geol. Soc. Am. Bull. 113 (2001) 825–836.

[15] G.M. Stock, R.S. Anderson, R.C. Finkel, Pace of landscape evolution in the Sierra Nevada, California, revealed by cosmogenic dating of cave sediments, Geology 32 (2004) 193–196.

[16] H.P. Schwarcz, W.J. Rink, Dating methods for sediments of caves and rockshelters with examples from the Mediterranean Region, Geoarcheology 16 (2001) 355–371.

[17] T.C. Partridge, D.E. Granger, M.W. Caffee, R.J. Clarke, Lower Pliocene hominid remains from Sterkfontein, Science 300 (2003) 607–612.

[18] M. Musgrove, J.L. Banner, L.E. Mack, D.M. Combs, E.W. James, H. Cheng, R.L. Edwards, Geochronology of Late Pleistocene to Holocene speleothems from central Texas: implications for regional paleoclimate, Geol. Soc. Am. Bull. 113 (2001) 1532–1543.

[19] I.D. Sasowsky, Determining the age of what is not there, Science 279 (1998) 1874.

[20] V.J. Polyak, W.C. McIntosh, N. Guven, P. Provencio, Age and origin of Carlsbad Cavern and related caves from ^{40}Ar/^{39}Ar of alunite, Science 279 (1998) 1919–1922.

[21] A.N. Palmer, Origin and morphology of limestone caves, Geol. Soc. Am. Bull. 103 (1991) 1–21.

[22] A.N. Palmer, Cave levels and their interpretation, Nat. Speleo. Soc. Bull. 49 (1987) 50–66.

[23] P. Bull, Some fine-grained sedimentation phenomena in caves, Earth Surf. Process. Landf. 6 (1981) 11–22.

[24] T.C. Atkinson, R.S. Harmon, P.L. Smart, A.C. Waltham, Palaeoclimate and geomorphic implications of ^{230}Th/^{234}U dates on speleothems from Britain, Nature 272 (1978) 24–28.

[25] P.W. Williams, Speleothem dates, Quaternary terraces and uplift rates in New Zealand, Nature 298 (1982) 257–260.

[26] M. Gascoyne, D.C. Ford, H.P. Schwarcz, Rates of cave and landform development in the Yorkshire Dales from speleothem age data, Earth Surf. Process. Landf. 8 (1984) 557–568.

[27] M. Gascoyne, H.P Schwarcz, Carbonate and sulphate precipitates, in: M. Ivanovich, R.S. Harmon (Eds.), Uranium Series Disequilibrium: Applications to Environmental Problems, Oxford Univ. Press, 1982, pp. 270–287.

[28] D.A. Richards, J.A. Dorale, Uranium-series chronology and environmental applications of speleothems, in: B. Bourdon, S. Turner, G. Henderson, C.C. Lundstrom (Eds.), Uranium Series Geochemistry, Rev. Mineral. Geochem., 2003, pp. 407–460.

[29] J.A. Dorale, R.L. Edwards, E.C. Alexander Jr., C. Shen, D.A. Richards, H. Cheng, Uranium-series dating of speleothems: current techniques, limits, and applications, in: I.D. Sasowsky,

J. Mylroie (Eds.), Studies of Cave Sediments, Kluwer Academic, New York, 2004, pp. 177–197.
[30] J. Cheng, R.L. Edwards, J. Hoff, C.D. Gallup, D.A. Richards, Y. Asmeron, The half-lives of uranium-234 and thorium-230, Chem. Geol. 169 (2000) 17–33.
[31] J. Lundberg, D.C. Ford, C.A. Hill, A preliminary U–Pb date on cave spar, Big Canyon, Guadalupe Mountains, New Mexico, J. Caves Karst Stud. 62 (2000) 144–146.
[32] A. Baker, D.C. Ford, P.L. Smart, Northwest European paleoclimate as indicated by growth frequency variations of secondary calcite deposits, Palaeogeogr. Palaeoclimatol. Palaeoecol. 100 (1993) 91–101.
[33] P. Bosak, P. Pruner, J. Kadlec, Magnetostratigraphy of cave sediments: application and limits, Stud. Geophys. Geod. 47 (2003) 301–330.
[34] V.A. Schmidt, Magnetostratigraphy of sediments in Mammoth Cave, Kentucky, Science 217 (1982) 827–829.
[35] F.G. Luiszer, Speleogenesis of Cave of the Winds, Manitou Springs, Colorado, in: I.D. Sasowsky, M.V. Palmer (Eds.), Breakthroughs in Karst Geomicrobiology and Redox Geochemistry, Karst Waters Inst., 1994, pp. 91–109.
[36] S.C. Cande, D.V. Kent, Revised calibration of the geomagnetic polarity time scale for the late Cretaceous and Cenozoic, J. Geophys. Res. 100 (1995) 6093–6095.
[37] D. Lal, Cosmic ray labeling of erosion surfaces: in situ nuclide production rates and erosion models, Earth Planet. Sci. Lett. 104 (1991) 424–439.
[38] D.E. Granger, P.F. Muzikar, Dating sediment burial with in situ-produced cosmogenic nuclides: theory, techniques, and limitations, Earth Planet. Sci. Lett. 188 (2001) 269–281.
[39] J. Masarik, R.C. Reedy, Terrestrial cosmogenic nuclide production systematics calculated from numerical simulations, Earth Planet. Sci. Lett. 136 (1995) 381–395.
[40] E.T. Brown, R.F. Stallard, M.C. Larsen, G.M. Raisbeck, F. Yiou, Denudation rates determined from the accumulation of in situ-produced cosmogenic nuclides, Earth Planet. Sci. Lett. 124 (1995) 19–33.
[41] T.L. Norris, A.J. Gancarz, D.J. Rokop, K.W. Thomas, Half-life of ^{26}Al: proceedings of the fourteenth lunar and planetary science conference: Part I: J. Geophys. Res. 88 (1983) B331–B333.
[42] R. Middleton, L. Brown, B. Dezfouly-Arjomandy, J. Klein, On ^{10}Be standards and the half-life of ^{10}Be, Nucl. Instrum. Methods Phys. Res., B Beam Interact. Mater. Atoms 82 (1995) 399–403.
[43] D.M. Anthony, D.E. Granger, A Late Tertiary origin for multilevel caves along the western escarpment of the Cumberland Plateau, Tennessee and Kentucky, established by cosmogenic ^{26}Al and ^{10}Be, J. Caves Karst Stud. 66 (2004) 46–55.
[44] R.L. Edwards, J.H. Chen, G.J. Wasserburg, ^{238}U–^{234}U–^{230}Th–^{232}Th systematics and the precise measurement of time over the past 500,000 years, Earth Planet. Sci. Lett. 81 (1987) 175–192.
[45] J.D.A. Zijderveld, A.C. demagnetization of rocks: analysis of results, in: D.W. Collinson, K.M. Creer, S.K. Runcorn (Eds.), Methods in Paleomagnetism, Elsevier, Amsterdam, 1967, pp. 254–286.
[46] J.L. Kirschvink, The least-squares line and plane and the analysis of paleomagnetic data, J. R. Astron. Soc. 62 (1980) 699–718.
[47] R.A. Fisher, Dispersion on a sphere, Proc. Royal Soc. Lond. 217 (1953) 295–305.
[48] C.P. Kohl, K. Nishiizumi, Chemical isolation of quartz for measurement of in-situ-produced cosmogenic nuclides, Geochim. Cosmochim. Acta 56 (1992) 3583–3587.
[49] J.O. Stone, A rapid fusion method for the extraction of Be-10 from soils and silicates, Geochim. Cosmochim. Acta. 62 (1998) 555–561.
[50] G. Balco, J.O.H. Stone, C. Jennings, Dating Plio–Pleistocene glacial sediments using the cosmic-ray produced radionuclides ^{10}Be and ^{26}Al, Am. J. Sci. 305 (2005) 1–41.
[51] D.E. Granger, J.W. Kirchner, R.C. Finkel, Spatially averaged long-term erosion rates measured from in situ-produced cosmogenic nuclides in alluvial sediment, J. Geol. 104 (1996) 249–257.
[52] C.S. Riebe, J.W. Kirchner, D.E. Granger, R.C. Finkel, Erosional equilibrium and disequilibrium in the Sierra Nevada, California, inferred from ^{26}Al and ^{10}Be in alluvial sediment, Geology 28 (2000) 803–806.
[53] J.O. Stone, Air pressure and cosmogenic isotope production, J. Geophys. Res. 105 (2000) 23753–23759.
[54] B. Heisinger, D. Lal, A.J.T. Jull, S. Kubik, S. Ivy-Ochs, K. Knie, E. Nolte, Production of selected cosmogenic radionuclides by muons: 2. Capture of negative muons, Earth Planet. Sci. Lett. 200 (2002) 357–369.